ASTRONOMY
AND
ASTROPHYSICS

ISO deep far-infrared survey in the "Lockman Hole"

II. Power spectrum analysis: evidence of a strong evolution in number counts[⋆,⋆⋆]

H. Matsuhara[1], **K. Kawara**[2], **Y. Sato**[1], **Y. Taniguchi**[3], **H. Okuda**[1], **T. Matsumoto**[1], **Y. Sofue**[2], **K. Wakamatsu**[4], **L.L. Cowie**[5], **R.D. Joseph**[5], and **D.B. Sanders**[5]

[1] The Institute of Space and Astronautical Science (ISAS), 3-1-1 Yoshinodai, Sagamihara, Kanagawa, 229-8510, Japan
[2] Institute of Astronomy, The University of Tokyo, 2-21-1 Osawa, Mitaka, Tokyo, 181-8588, Japan
[3] Astronomical Institute, Tohoku University, Aoba, Sendai 980-8578, Japan
[4] Faculty of Engineering, Gifu University, Gifu 501-1193, Japan
[5] Institute for Astronomy, University of Hawaii, 2680 Woodlawn Drive, Honolulu, HI 96822, USA

Abstract. We investigate the characteristics of FIR brightness fluctuations at $90\,\mu$m and $170\,\mu$m in the Lockman Hole, which were surveyed with ISOPHOT aboard the Infrared Space Observatory (ISO). We first calculated the angular correlation function of each field and then its Fourier transform (the angular Power Spectral Density: PSD) over the spatial frequency range of $f = 0.05$–$1\,\mathrm{arcmin}^{-1}$. The PSDs are found to be rather flat at low spatial frequencies ($f \leq 0.1\,\mathrm{arcmin}^{-1}$), slowly decreasing toward higher frequencies. These spectra are unlike the power-law ones seen in the IR cirrus fluctuations, and are well explained by randomly distributed point sources. Furthermore, point-to-point comparison between $90\,\mu$m and $170\,\mu$m brightness shows a linear correlation between them, and the slope of the linear fit is much shallower than that expected from the IR cirrus color, and is consistent with the color of galaxies at low or moderate redshift ($z < 1$). We conclude that the brightness fluctuations in the Lockman Hole are not caused by the IR cirrus, but are most likely due to faint star-forming galaxies. We also give the constraints on the galaxy number counts down to 35 mJy at $90\,\mu$m and 60 mJy at $170\,\mu$m, which indicate the existence of a strong evolution down to these fluxes in the counts. The galaxies responsible for the fluctuations also significantly contribute to the cosmic infrared background radiation.

Key words: galaxies: evolution – galaxies: starburst – cosmology: observations – infrared: ISM: continuum – infrared: galaxies

1. Introduction

In order to understand the history of galaxy formation and evolution, surveys at far-infrared (FIR) and submillimeter wavelengths are essentially important, since a large portion of star formation activity in the universe may be hidden by dust, prohibiting optical and near-infrared studies due to the enormous extinction. The recent detection of the far-infrared Cosmic Infrared Background (CIB) radiation by COBE, which appears to have comparable brightness to the total intensity in deep optical counts from the Hubble deep field (Fixen et al. 1998; Hauser et al. 1998; Lagache et al. 2000), indicates that the infrared-bright galaxies are responsible for roughly half of the energy released by nucleosynthesis. Various discrete source surveys are also being pursued from mid-infrared to submillimeter wavelengths. For example, source counts at $15\,\mu$m (Aussel et al. 1998; Altieri et al. 1998; Elbaz et al. 1999), at $170\,\mu$m (Kawara et al. 1998 (paper I); Puget et al. 1999), and at $850\,\mu$m (Blain et al. 1999) have been reported. Using both CIB and these new number count data, modeling of the cosmic star formation history has been attempted by many authors (Guiderdoni et al. 1998; Dwek et al. 1998; Rowan-Robinson 1999; Tan et al. 1999; Ishii et al. 1999). All of them require a strong evolution in the star formation rate as we look back to high redshift (more than 10 times larger at $z \simeq 1$).

Although the FIR deep survey is now considered a key observing method for the exploration of the "optically dark side" of the star formation history of galaxies (Guiderdoni et al. 1997), the detectivity of 1m-class space FIR telescopes is likely to be limited by the noise due to the fluctuation of the IR cirrus (Low et al. 1984), emission from the interstellar dust, even at high Galactic latitude (Helou & Beichman 1990). Hence a detailed study of the IR cirrus fluctuations is highly important, especially for the planning of the deep surveys intended with forthcoming IR space telescopes such as ASTRO-F(IRIS) (Murakami 1998) and SIRTF (Fanson et al. 1998).

The spatial structure of the IR cirrus at $100\,\mu$m as measured by IRAS was extensively studied by Gautier et al. (1992) and

Abergel et al. (1996). From a Fourier analysis of the brightness distribution, Gautier et al. found that the Power Spectral Density (PSD) of the brightness fluctuation at $100\,\mu$m follows a power-law function of the spatial frequency with an index of about 3 below the spatial frequency corresponding to the IRAS beam size (about $0.25\,\mathrm{arcmin}^{-1}$). They also found that the PSD is proportional to B_0^3, where B_0 is the mean brightness of the IR cirrus. The ISOPHOT (Lemke et al. 1996) onboard the ISO (Kessler et al. 1996) is capable of observing the IR cirrus at wavelengths longer than $100\,\mu$m, with a better spatial resolution than that of IRAS. Herbstmeier et al. (1998) analyzed the spatial character-istics of four fields measured by ISOPHOT, and obtained similar power-law spectra for relatively bright cirrus regions. Recently Lagache & Puget (2000) have made a power spectrum analysis of the $170\,\mu$m image of the Marano 1 field, and found a signif-icant excess at $f = 0.25$–$0.6\,\mathrm{arcmin}^{-1}$, which they attributed to the fluctuations due to unresolved extra-galactic sources.

In this paper we investigate the characteristics of FIR bright-ness fluctuations in the Lockman Hole, a region with a uniquely low HI column density (Lockman et al. 1986), and thus minimal IR cirrus contribution to the fluctuations. Therefore the fluctua-tions in the Lockman Hole are likely to be dominated by faint, distant galaxies (Helou & Beichman 1990; Herbstmeier et al. 1998) and the fluctuation analysis of FIR images will provide unique information on the number counts of infrared galaxies even below the source-confusion limit, thus constraining the parameters characterizing the number count models.

This paper is organized as follows: Sect. 2 briefly describes the observations and data processing. Sect. 3 explains the power spectrum analysis and examines the contribution by the IR cirrus fluctuations and also describes a simulation of the images and the PSDs. Sect. 4 describes the constraints on the galaxy number counts. The nature of the sources responsible for the fluctuations is discussed in Sect. 5, and Sect. 6 gives the conclusions.

2. Observation and data processing

The FIR survey of the Lockman Hole, which was executed as a part of Japan/UH cosmology program using the ISAS guar-anteed time, is described in Taniguchi et al. (1994) and paper I. Two $44' \times 44'$ fields named LHEX and LHNW were mapped with two filters: C_90 (centered at $90\,\mu$m) and C_160 ($170\,\mu$m). Each of the two fields is made up of 4 sub-fields.

Each sub-field map was produced from the edited raw data by the PHT Interactive Analysis (PIA; Gabriel et al. 1997) ver-sion 7.1 or 7.2, and is hereafter referred to as an AAP (As-tronomical Analysis Processing of PIA) map. Each AAP map is either 58×58 pixels ($23''$/pixel) for a $90\,\mu$m sub-field, or 31×31 pixels ($46''$/pixel) for a $170\,\mu$m sub-field. To correct the drift in the responsivity of the detectors, we applied the median filter smoothing (see Paper I for details) to the AAP data.

Together with the final AAP maps we also produced the uncertainty maps, and found that the typical 3σ noise is as low as 0.012MJy/sr (0.60mJy/pixel for a $46''\times46''$ pixel), indicating that the instrumental noise is negligible in the following results.

As was done in Paper I, the observed fluxes as well as the brightness of the images are scaled based on the fluxes of the brightest source F10507+5723 (UGC 06009) measured with IRAS. We found that the flux calibration based on the FCS1 mea-surements underestimates the $90\,\mu$m flux of the IRAS source by a factor of 2.6, although it gives the mean brightness of the im-ages consistent with the COBE/DIRBE brightness within 25 per cent. The $170\,\mu$m flux of the IRAS source is assumed to be 1133 mJy as described in Paper I. The flux calibration based on the FCS1 measurements again underestimates the $170\,\mu$m flux by a factor of 1.5. For the $170\,\mu$m flux, we found that the discrepancy is mostly due to an underestimate of the effective solid angle of the ISOPHOT detector. Puget et al. (1999) and Lagache & Puget (2000) used an effective solid angle at $170\,\mu$m derived from Saturn footprint measurements, which is signifi-cantly larger than that used in the PIA. Here we assume theoreti-cal PSFs of a telescope with a 60 cm primary mirror and a 20 cm secondary mirror which agree well with those measured during the ISOPHOT calibration observations (Müller 2000). With this assumption, the factors of 2.6 ($90\,\mu$m) and 1.5 ($170\,\mu$m) discrep-ancies reduce to factors of 2.0 ($90\,\mu$m) and 1.2 ($170\,\mu$m). The origin of the residual discrepancies is still unknown. However, this is not problematic for the main results and conclusions of this paper as described in Sects. 4 and 5 as long as the fluxes of F10507+5723 determined by the IRAS faint source survey are correct.

Fig. 1 shows the images of LHEX and LHNW used for the fluctuation analysis, each of which is the largest square area extracted from the mosaiced map (see Fig. 3 of Paper I) made up from four sub-field AAP maps. Each image is rebinned into 103×103 pixels^2 (C_90), 53×53 pixels^2 (C_160 LHEX), or 51×51 pixels^2 (C_160 LHNW). The plate scale is $23''$/pixel for $90\,\mu$m maps, and $46''$/pixel for $170\,\mu$m maps.

3. The power spectra and the simulation

For each image shown in Fig. 1 the 2-dimensional angular cor-relation function $C(x,y)$ was calculated from the brightness distribution $B(x_0,y_0)$:

$$C(x,y) = <(B(x_0,y_0) - \bar{B})(B(x_0 + x, y_0 + y) - \bar{B})> \quad (1)$$

where bracket $<>$ represents the average over the whole area in each image shown in Fig. 1, and $\bar{B} = <B>$. Then, the co-ordinates were expressed in polar coordinates as $C(r,\theta)$, and the Fourier transforms in various radial directions were calcu-lated (*i.e.* θ is fixed for each transform). One-dimensional power spectral density (PSD) $P(f)$ is calculated from

$$P(f) = \frac{2}{N}\sum_{k=0}^{N-1} C_k cos(2\pi f r_k)\,, \quad (2)$$

where f is spatial frequency ($1/(Nr_{\mathrm{pix}}) \leq f \leq 1/(2r_{\mathrm{pix}})$), $r_k \equiv r_{\mathrm{pix}}k$ ($k = 0, 1, \cdots, N-1$), r_{pix} is the pixel size of the map, Nr_{pix} is the largest angular size for which the angular cor-relation function is evaluated, and $C_k \equiv C(r = r_k, \theta)$. Note that the units of the PSDs are the same as that of the angular
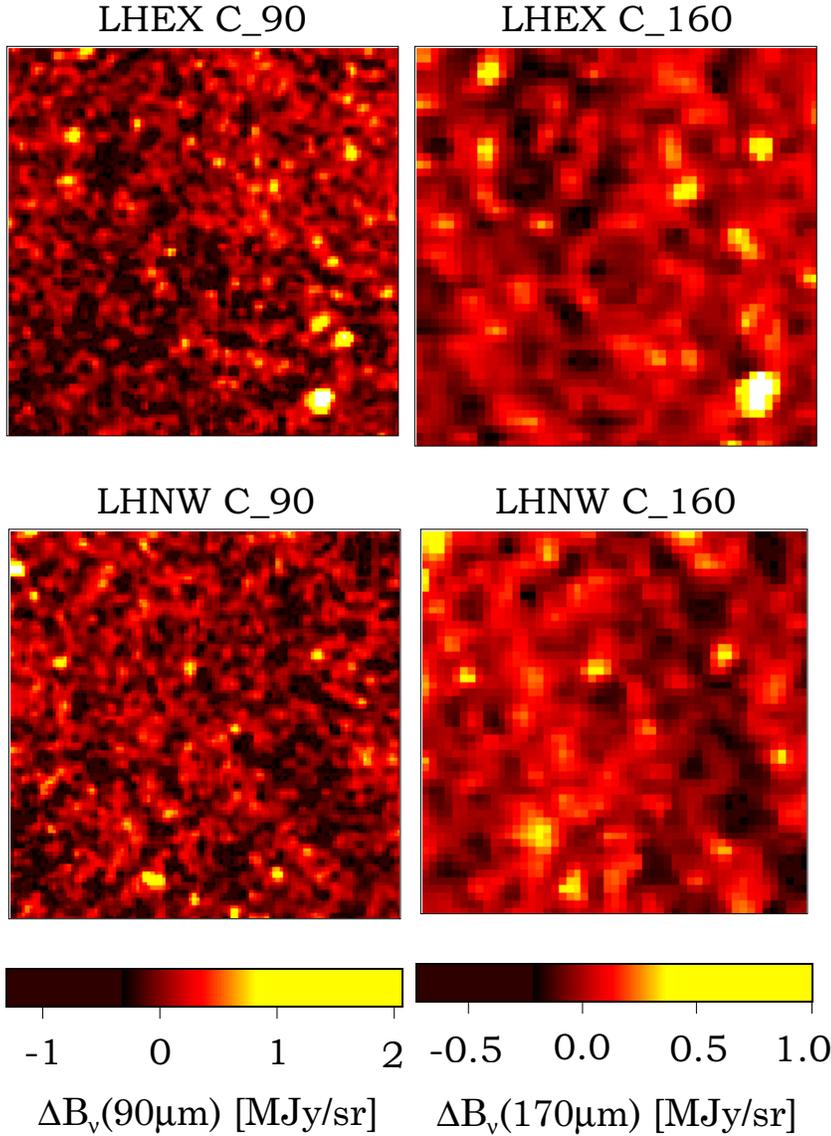
LHEX C_90

LHEX C_160

LHNW C_90

LHNW C_160

$\Delta B_\nu(90\mu m)$ [MJy/sr]

$\Delta B_\nu(170\mu m)$ [MJy/sr]

Fig. 1. The left column shows $90\,\mu$m images of LHEX (top) and LHNW (bottom). Each image is $39'.5 \times 39'.5$ wide ($23''$/pixel). The right column shows $170\,\mu$m images ($46''$/pixel). The LHEX image is $40'.6 \times 40'.6$ wide, while the LHNW one is $39'.1 \times 39'.1$ wide. The brightness shown in each image is offset from its median brightness. Each image is made of four $22' \times 22'$ sub-fields. Roughly the north is left and the west is top.

correlation function: $\mathrm{Jy}^2/\mathrm{sr}^2$. Finally, the PSDs were averaged with respect to θ and are shown in Fig. 2. It is noteworthy that the fluctuations at high frequencies ($f \geq 0.8$ arcmin^{-1} for 90 μm, and $f \geq 0.4$ arcmin^{-1} for 170 μm) are smoothed by the instrumental beam and therefore the PSDs decrease appreciably. The small error bars of PSDs represent the standard deviation among a set of the PSDs with different θ, showing that the PSDs are almost independent of θ.

In order to check the contributions from bright sources, the PSDs are derived by masking circular regions with a $4\times$FWHM diameter around bright sources with fluxes above $S_{\max}$: $S_{\max} = 250$ mJy at 170 μm[1], $S_{\max} = 150$ mJy at 90 μm. In the following the resultant PSDs are called "residual PSDs", and are also shown in Fig. 2. Interestingly, the residual PSD for each image is more than half of the PSD of corresponding original image with almost the same spectral shape, indicating that there re-

mains significant contribution from randomly distributed point sources with fluxes below $S_{\max}$.

In Fig. 2 typical IR cirrus PSDs are also compared in order to check the contribution of the IR cirrus to the PSDs of the Lockman Hole[2]. We examined several IRAS 100 μm maps of high-latitude clouds in Ursa Major ($l = 145°$, $b = 40°$), which are reproduced from the IRAS Sky Survey Atlas (ISSA) by reducing the brightness by a factor of 0.72, following the COBE/DIRBE calibration (Wheelock et al. 1994). The average brightness of the cirrus is 2–3 MJy/sr, and each map is $150' \times 150'$ wide with $1'.5$/pixel. The derived PSDs show a power-law distribution with an index of -1.5. Gautier et al. (1992) noted that one-dimensional analysis of the IR cirrus yielded spectral indices near -2. These cirrus fluctuation spectra are much differ-

---

[1] As for 170 μm images, smaller values of $S_{\max}$ significantly reduce the amount of residual images.

[2] The formula for the IR cirrus PSD by Gautier et al. (1992) cannot be directly compared with the present work, because the power spectrum analysis presented here is one-dimensional one while the formula of Gautier et al. is based on the two-dimensional analysis.
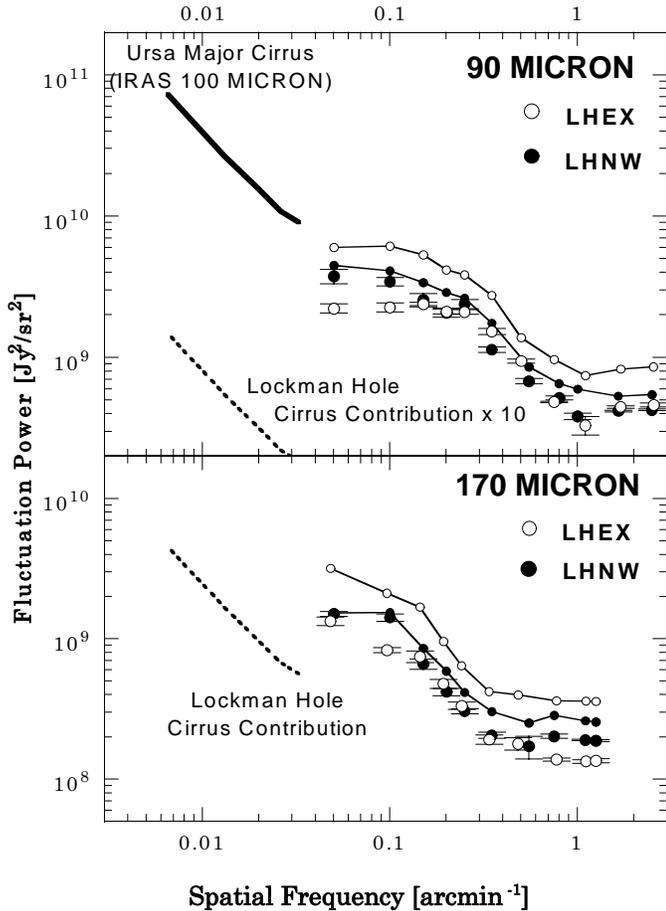
Fig. 2. Fluctuation power spectral densities (PSDs) of 90 μm (top) and 170 μm (bottom) images. Open circles represent PSDs of LHEX and filled circles represent PSDs of LHNW. As well as the PSDs of the original images (Fig. 1) shown by circles connected by thin-solid lines, the PSDs of the residual images ("residual PSDs"), where the pixels containing bright sources above 150 mJy (90 μm), 250 mJy (170 μm) are masked, are also shown by circles alone. The brightest source (IRAS F10597+5723) located in LHEX significantly contributes to the PSDs of the LHEX images. The 1σ error bars, shown only for the residual PSDs, represent the standard deviation in a set of the PSDs with different position angles in the sky. Thick line is an example of the IR cirrus PSD, which is an average spectrum of several IR cirrus in Ursa Major, with 100 μm brightness of 2–3 MJy/sr. Dotted lines are the IR cirrus PSDs in the Lockman Hole, estimated by assuming that the cirrus PSDs are proportional to B_0^3, where B_0 is mean brightness of the cirrus cloud.

ent from those obtained for the Lockman Hole images at 90 μm, which show rather flat spectra at lower spatial frequencies. The 170 μm spectra present a slope similar to the IR cirrus one, but this can be explained by the shape of the footprint power spectrum of ISOPHOT detectors. Moreover, the fluctuation powers are much larger than those estimated for the IR cirrus, which are also shown in Fig. 2. We assume that the cirrus PSD is proportional to B_0^3 (Gautier et al. 1992), and taking the mean brightness B_0 of the IR cirrus in the Lockman Hole as 0.33 MJy/sr at 90 μm and 1.0 MJy/sr at 170 μm. These values are estimated from the

atomic hydrogen column density of 6×10^{19} atoms cm^{-2} in LHEX (Jahoda et al. 1990) and the COBE/DIRBE data analysis in the Lockman Hole by Lagache et al. (1999, in their Table 4). We can conclude that the IR cirrus contribution to the PSDs in the Lockman Hole is negligible over all spatial frequencies $f \geq 0.05$.

In the following we interpret the residual PSDs in terms of unresolved point sources, probably galaxies. We neglect the spatial correlation between galaxies, thus assuming that galaxies are randomly distributed in the images. Then the residual PSD will be the product of the footprint power spectrum of the ISOPHOT detector and the fluctuation power due to the point sources, which is a white power spectrum given by:

$$P_{\text{source}} = \int_{S_{\text{min}}}^{S_{\text{max}}} S^2 \frac{dN}{dS} dS \qquad (3)$$

where dN/dS is differential source counts. From the residual PSDs observed, we derive $P_{\text{source}} = 13000 \pm 3000\,\text{Jy}^2/\text{sr}$ at 90 μm ($S_{\text{max}} = 150$ mJy) and $P_{\text{source}} = 12000 \pm 2000\,\text{Jy}^2/\text{sr}$ at 170 μm ($S_{\text{max}} = 250$ mJy), where the errors do not include systematic ones due to uncertainties in the flux calibration. Lagache & Puget (2000) reported the detection of $P_{\text{source}} = 7400\,\text{Jy}^2/\text{sr}$ at 170 μm for the Marano 1 field, after sources brighter than 100 mJy are removed. Contribution from detected sources with fluxes between 100 mJy and 250 mJy is estimated to be about 7000 Jy^2/sr. Thus the fluctuation power in the Lockman Hole due to the sources fainter than 100 mJy is $\sim 5000\,\text{Jy}^2/\text{sr}$, which is comparable to that observed in the Marano 1 field.

A simulation was performed by making 90 μm and 170 μm images made up only by galaxies with fluxes between S_{min} and S_{max} and calculating their PSDs. Here galaxies are treated as point sources with a PSF specific to the respective wavelength band of ISOPHOT. We used the image of the bright IRAS source (F10507+5723) seen in LHEX images as the PSF. The number of sources and their flux densities are controlled by the source counts. We examined the non-evolution count model by Takeuchi et al. (1999) and the scenario E by Guiderdoni et al. (1998). We assume $S_{\text{min}} = 10$ mJy because the fluctuations due to galaxies fainter than 10 mJy are negligible in case of these models. The resulted PSDs are compared with the residual PSDs in Fig. 3. These simulated PSDs are not sufficient to explain the observed PSDs although the spectral shapes are quite similar.

4. Constraints on the number counts

In this section we will investigate the source counts below S_{max}, by fitting the simulated PSDs to the residual PSDs. In Paper I we presented the number density of sources brighter than 150 mJy at both filter bands. After Paper I was published, the data processing and the source extraction technique have been improved, and now we obtained source number counts down to $S = 70$ mJy at 90 μm and $S = 100$ mJy at 170 μm, although the counts at such low fluxes may be overestimated due to the source confusion. We found that the cumulative counts above 150 mJy show
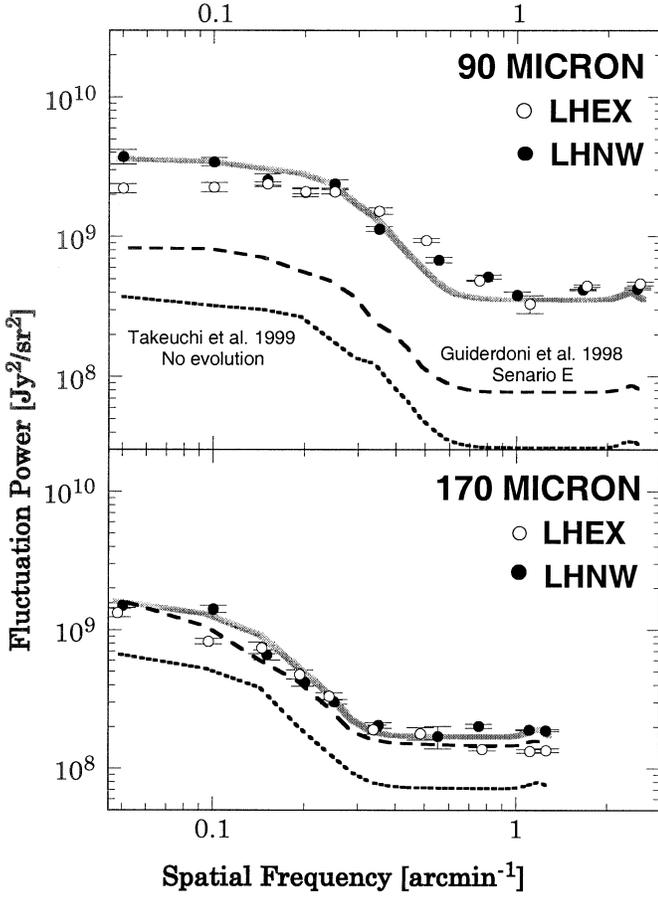
Fig. 3. The residual PSDs of $90\,\mu$m (top) and $170\,\mu$m (bottom) images (open circles and filled circles, same as Fig. 2) are compared with the simulated PSDs based on various number counts models: dashed lines are PSDs of the simulated images by Guiderdoni et al. (1998) scenario E, while the dotted lines are those by Takeuchi et al. (1999) no-evolution. Thick gray lines are examples of the simulated images produced by simple double power-law number count models (see text for details).

quite a steep increase as the source flux decreases: $\beta \simeq 3$ where $N(>S) \propto S^{-\beta}$. These results will be described in detail in Paper III by Kawara et al. (in preparation). If β remains equal to -3 down to $S_{\min} = 1\,$mJy, then the fluctuation power (P_{source}) calculated by Eq. (3) exceeds the observed ones by an order of magnitude. Hence at a certain flux below $S_{\max}$, we expect that the slope of the counts must flatten to $\beta < 2$ so that the predicted fluctuations do not exceed the observed ones. We thus considered simple double power-law count models and evaluated the simulated PSDs: in the flux range $S_{\max} \geq S \geq S_{\text{crit}}$

$$N(>S) = N_{\max} \left(\frac{S}{S_{\max}} \right)^{-\beta_0} , \qquad (4)$$

and in flux range $S_{\text{crit}} \geq S \geq S_{\min}$

$$N(>S) = N_{\text{crit}} \left(\frac{S}{S_{\text{crit}}} \right)^{-\beta_1} , \qquad (5)$$

Table 1. Number count parameters

band	$S_{\max}$ [Jy]	$N_{\max}$ [sources/sr]	uncertainty in $N_{\max}$
$90\,\mu$m	0.15	1.4×10^5	$+16\%, -47\%$
$170\,\mu$m	0.25	5.4×10^4	$+24\%, -44\%$

where $N_{\text{crit}} = N_{\max}(S_{\text{crit}}/S_{\max})^{-\beta_0}$, and β_0, β_1 are assumed to obey inequalities $0 \leq \beta_1 < \beta_0 \leq 4$. $N_{\max}$ and its uncertainty are listed in Table 1. The uncertainty in $N_{\max}$ includes Poisson uncertainties based on the total number of sources with flux above $S_{\max}$ in all images, and systematic ones originating from the incompleteness due to the source confusion, which will be discussed in paper III. If $\beta_1 < 2 < \beta_0$, the simulated PSD is not sensitive to $S_{\min}$ and is dominated by sources with fluxes around S_{crit}, as discussed in Lagache and Puget (2000). Various sets of parameters can be chosen so that the simulated PSDs fit to the residual PSDs. Examples of the simulated PSDs which fit well to the residual PSDs are also shown in Fig. 3, for which $\beta_0 = 3.0$, $\beta_1 = 1.0$ for both $90\,\mu$m and $170\,\mu$m counts, and $S_{\text{crit}} = 80$ mJy for $90\,\mu$m counts and $S_{\text{crit}} = 150$ mJy for $170\,\mu$m one. We found that the simulated PSDs can fit the residual PSDs over all spatial frequencies within ± 22 per cent for the $90\,\mu$m PSDs and ± 17 per cent for the $170\,\mu$m ones. These deviations of the residual PSDs from the simulated PSDs are also included as uncertainties in the residual PSDs.

We now derive the allowed regions in plots of the cumulative counts at fluxes below $S_{\max}$. The bottom border of the allowed regions is derived by examining the single power-law counts $(S_{\text{crit}} = S_{\min} = 1\,\text{mJy})^3$ and we obtain $\beta_0 = 1.8$ for $90\,\mu$m counts and $\beta_0 = 1.7$ for $170\,\mu$m ones. In case of double power-law counts we may choose a larger value of β_0 with a set of parameter pairs $(S_{\text{crit}}, \beta_1)$, and among them S_{crit} for $\beta_1 = 0$ is the largest. Thus we determine the upper borders of the allowed regions by connecting $(S_{\text{crit}}, N_{\text{crit}})$ points of numerous models with $\beta_1 = 0$ and $\beta_0 = 2$–4. The results are shown by the shaded area in Fig. 4. As for the $170\,\mu$m counts, the bottom border of the allowed region is close to the Scenario E model by Guiderdoni et al. (1998), and is consistent with the counts at 120 mJy and at 200 mJy obtained from the FIRBACK Marano 1 survey (Puget et al. 1999). On the other hand, the allowed region for $90\,\mu$m counts are significantly above those of any currently existing models.

The bottom border derived here cannot be applied below a certain flux S_{L}, which is the flux at the intersection between an upper-border count model with the steepest slope ($\beta_0 = 4$, $\beta_1 = 0$), and the bottom border: $S_{\text{L}} = 30\,$mJy ($90\,\mu$m) or 50 mJy ($175\,\mu$m). By definition, the upper border model do not require sources below $S_{\text{crit}}(> S_{\text{L}})$. On the other hand, in case of the bottom border model, contribution to the fluctuations from sources below S_{L} is still appreciable, about half of the total. Considering the uncertainties in $N_{\max}$ and the residual PSDs

---

^{3} Lower value of $S_{\min}$ does not appreciably change the results: $\beta_0 = 1.7$ even if $S_{\min} = 0$.
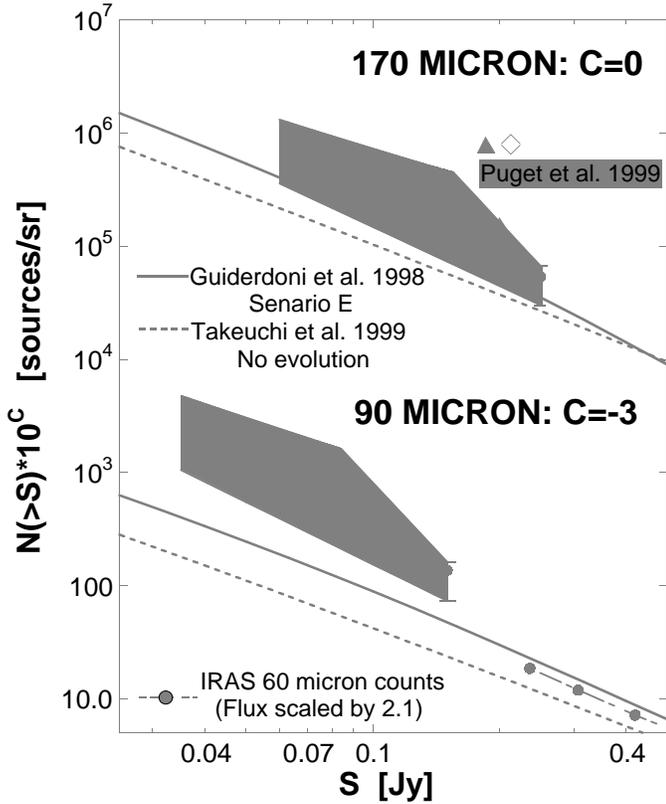
Fig. 4. The shaded areas show the allowed regions for various number count models, which are consistent with the fluctuation powers of the Lockman Hole images (Fig. 3). The bottom border is obtained from the simple number count model with a single power-law index between $S_{min} = 1$ mJy and $S_{max} = 150$ mJy (90 μm) or 250 mJy (170 μm). The upper border is determined from the allowed double power-law count models. See text for detailed information. The filled circles are observed number counts at S_{max}. The theoretical number count models by Guiderdoni et al. (1998) (scenario E: solid lines) and the no evolution model by Takeuchi et al. (1999) (dashed lines) are also shown. The open diamonds and triangles are observed and incompleteness-corrected source counts obtained by the FIRBACK Marano 1 survey (Puget et al. 1999). The open circles with dash-dotted line show the IRAS 60 μm counts, in which the flux is scaled by the factor $S_\nu(90\,\mu\mathrm{m})/S_\nu(60\,\mu\mathrm{m}) = 2.1$.

as discussed above, we finally give $S_L = 35$ mJy for 90 μm counts and $S_L = 60$ mJy for 170 μm counts.

5. Discussion

We attribute the origin of the residual PSDs to the random distributions of faint sources which can no longer be identified as individual sources due to the source confusion. Another piece of evidence which supports this interpretation is the 170 μm/90 μm brightness ratio of the FIR background emission. In Fig. 5 we show the point-to-point comparison between the 90 μm and the 170 μm sky brightness. Here we examine the residual images after masking pixels around the sources with $S > S_{max}$. In order to match the spatial resolution between 90 μm (76″ FWHM) and 170 μm (144″ FWHM) images, one wavelength band im-
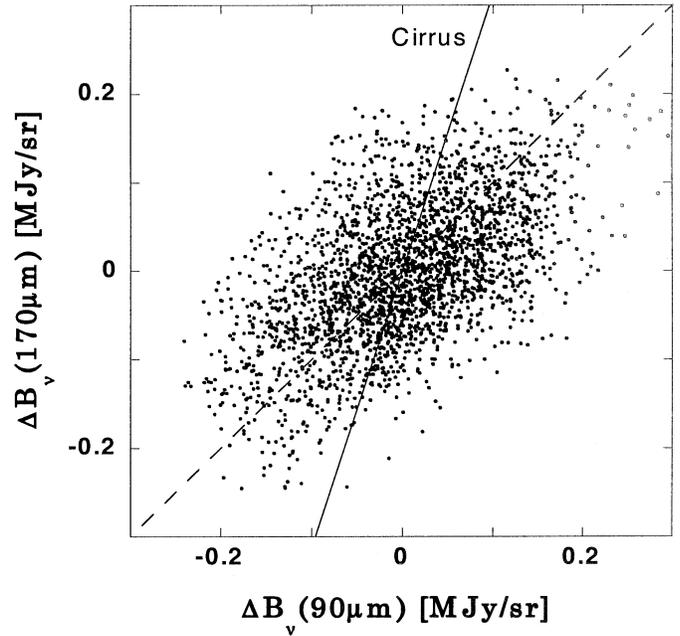

Fig. 5. Point-to-point comparison between the 90 μm sky brightness and the 170 μm one in the Lockman Hole. The brightness is not absolute one, but is offset from the median brightness. In this plot the pixels around the bright sources ($S \geq 150$mJy for 90 μm, $S \geq 250$mJy for 170 μm) are not shown. In order to avoid the error due to the difference of the beam size between the two bands, the 90 μm images are convoluted with the 170 μm beam profile (144″FWHM). The solid line showing the IR cirrus color vector is taken from Lagache et al. (1999), which is 17.5 K gray-body with an emissivity proportional to λ^{-2}.

age is convoluted with the other wavelength band beam profile. Although the scatter is large, the plot shows linear correlation with a slope of unity. This background color is quite different from that expected for the IR cirrus (about 3.1), and can be interpreted as a typical FIR color of galaxies contributing to the fluctuation. The fluctuation color due to faint galaxies depends on their redshift, and their SEDs. The relations between the FIR flux ratio and the redshift for SEDs of the cirrus dominated galaxy, the pure starburst galaxy (Efstathiou et al. 2000; Efstathiou & Siebenmorgen 2000), and the mixture of these two SEDs which represents a star-forming galaxy's SED like IRAS F10507+5723, are shown in Fig. 6. The flux ratio of $S_\nu(170\mu\mathrm{m})/S_\nu(90\mu\mathrm{m}) = 1$ is attained at $z \simeq 0.7$ for a pure starburst galaxy, while a cirrus dominated galaxy or a star-forming galaxy with a small contribution from starburst component must be local ($z \leq 0.1$).

From Fig. 6 we can also justify the flux calibration based on the IRAS fluxes of F10507+5723. If we adopt the ISO 90 μm flux determined by PIA and the theoretical PSFs, then $S_\nu(90\mu\mathrm{m})/S_\nu(60\mu\mathrm{m}) = 1.0$ which is the color of a pure-starburst galaxy, while the ISO flux ratio $S_\nu(170\mu\mathrm{m})/S_\nu(90\mu\mathrm{m}) = 1.6$ is much larger than that expected for any nearby ($z \simeq 0$) galaxies.

The local cirrus dominated galaxies are not likely to be the dominant sources responsible for the fluctuations, since such

galaxies are relatively bright at optical wavelength and hence the source number density in the Lockman Hole at optical wavelength would exceed the observed one by more than an order of magnitude: as shown in Table 1 we obtained source density of about 2×10^5 sources/sr (60 sources/deg^2) at $S \simeq 100$ mJy. Using the averaged SED of normal galaxies given by Schmidt et al. (1997), the B magnitude of a 100 mJy source at $90\,\mu$m is estimated to be about 16 mag. Reported B-band source counts above B = 16 mag is only a few sources per square degrees (Kirschner et al. 1979; Ellis 1983). Hence the galaxies responsible for the fluctuations must be heavily extincted at optical wavelengths, which is a well-known feature of starburst galaxies. In conclusion, the major source of the brightness fluctuations is most probably the star-forming galaxies located at $z < 1$ extincted at optical wavelengths.

In the plot of the $90\,\mu$m counts in Fig. 4, the IRAS counts are also plotted. These were originally the $60\,\mu$m counts, in which the flux is scaled by the factor $S_\nu(90\,\mu m)/S_\nu(60\,\mu m)$=2.1. This scaling factor is derived by the IRAS source counts at relatively high fluxes ($S_\nu(100\,\mu m) > 1$ Jy) (Rowan-Robinson et al. 1986), and is consistent with the color of normal galaxies with a partial contribution from starburst. Thus, if such galaxies dominate the $60\,\mu$m counts down to 110 mJy, this scaling is valid. We used the complete differential source counts down to 110 mJy by Lonsdale et al. (1990) and Bertin et al. (1997), and as shown in Fig. 4 the scaled counts are in good agreement with the model counts given by Guiderdoni et al. (1998). Since the integrated counts down to 150 mJy is much larger than the model counts, the integrated counts must show a steep rise between 150 mJy and 240 mJy, which, however, could not be observed in the IRAS $60\,\mu$m counts due to the source confusion (Hacking & Houck 1987). Further studies from space like ASTRO-F and SIRTF will judge if this steep rise is real.

Finally, we mention on the impact of the present work to the cosmic infrared background (CIB). Hauser et al. (1998) reported an upper limit of 1.1 MJy/sr at $100\,\mu$m and a positive detection of the CIB of 1.2 MJy/sr at $140\,\mu$m and 1.1 MJy/sr at $240\,\mu$m. Lagache et al. (1999) reported lower values of the CIB: 0.72 ± 0.30 MJy/sr at $140\,\mu$m and 0.91 ± 0.15 MJy/sr at $240\,\mu$m by further subtracting the dust emission associated with the diffuse ionized gas. Lagache et al. (2000) also reported the CIB at $100\,\mu$m: 0.78 ± 0.21 MJy/sr. By summing the fluxes of all detected sources above 150 mJy, we obtained an integrated brightness of the CIB of 0.031 MJy/sr at $90\,\mu$m and 0.050 MJy/sr at $170\,\mu$m. If we consider the constraints on the number counts for $S \geq S_L$ shown in Fig. 4, then the integrated brightness would be 0.09 – 0.30 MJy/sr at $90\,\mu$m for sources above 35 mJy and 0.053–0.15 MJy/sr at $170\,\mu$m for source above 60 mJy. Hence, 5–40 per cent of CIB can now be attributed to the integrated light of discrete sources above S_L which are responsible for the fluctuations.

6. Conclusion

We have studied the characteristics of FIR brightness fluctuations at $90\,\mu$m and $170\,\mu$m in the Lockman Hole, using the
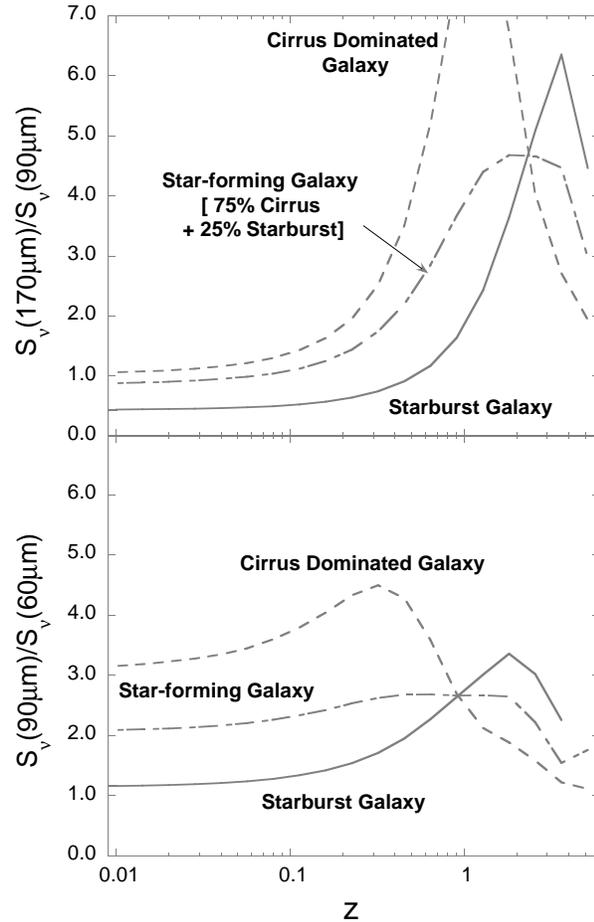

Fig. 6. FIR color vs redshift (z) relation for the cirrus dominated galaxy and the starburst galaxy. (Top) the ratio of $S_\nu(170\,\mu m)$ to $S_\nu(90\,\mu m)$, (bottom) the ratio of $S_\nu(90\,\mu m)$ to $S_\nu(60\,\mu m)$. The model FIR SEDs are taken from Efstathiou et al. (2000) and Efstathiou & Siebenmorgen (2000). The dash-dotted lines represent the color-z relation of an example of the mixed SED, cirrus: starburst = 0.75: 0.25 at $100\,\mu$m.

power spectrum analysis over the spatial frequency range of $f = 0.05 - 1$ arcmin^{-1}. The spectra of PSDs are found to be rather flat at low frequencies, which differs from that expected for IR cirrus fluctuations. We interpret the spectral characteristics of PSDs as those of randomly distributed point sources. The fluctuations in the Lockman Hole are not dominated by the IR cirrus, and are instead most likely due to star-forming galaxies. We next showed the constraints on the galaxy number counts down to 35 mJy at $90\,\mu$m and 60 mJy at $170\,\mu$m, assuming that only galaxies contribute to the observed fluctuation powers. This analysis indicates the existence of steep rise in the integrated counts down to these fluxes and especially at $90\,\mu$m, the source density is much larger than that expected from the currently available number count models.

We also found a linear correlation between sky brightnesses at $90\,\mu$m and $170\,\mu$m, even if pixels around the bright sources are masked from the images. The slope of the linear fit is much lower than the color of the IR cirrus, indicating that the point sources are star-forming galaxies at low or moderate redshift

($z < 1$). These galaxies with fluxes above 35 mJy or 60 mJy also significantly contribute to the CIB recently reported by Hauser et al. (1998) and Lagache et al. (2000).

References

Abergel A., Boulanger F., Delouis J.M., Dudziak G., Steindling S., 1996, A&A 309, 245

Altieri B., Metcalfe L., Kneib J.P., et al., 1998, A&A 343, L65

Aussel H., Cesarsky C.J., Elbaz D., Starck J.L., 1998, A&A 342, 313

Bertin E., Dennefeld M., Moshir M., 1997, A&A 323, 685

Blain A.W., Kneib J.-P., Ivison R.J., Smail I., 1999, ApJ 512, L87

Dwek E., Arendt R.G., Hauser M.G., et al., 1998, ApJ 508, 106

Efstathiou A., Rowan-Robinson M., Siebenmorgen R., 2000, A&A in press

Efstathiou A., Siebenmorgen R., 2000, in preparation

Elbaz D., Cesarsky C.J., Fadda D., et al., 1999, A&A 351, L37

Ellis R.S., 1983, In: Jones B.J.T., Jones J.E.(eds.) The Origin and Evolution of Galaxies. D. Reidel, p. 255

Fanson J., Fazio G., Houck J., et al., 1998, Proc. SPIE 3356, 478

Fixen D.J., Dwek E., Mather J.C., Bennet C.L., Shafer R.A., 1998, ApJ 508, 123

Gabriel C., Acosta-Pulido J., Henrichsen I., et al., 1997, In: Hunt G., Payne H.E. (eds.) Proc. of the ADASS VI conference, ASP conference series vol. 125, p. 108

Gautier T.N., Boulanger F., Pérault M., Puget J.-L., 1992, AJ 103, 1313

Guiderdoni B., Bouchet F.R., Puget J.-L, Guilaine G., Hivon E., 1997, Nat 390, 257

Guiderdoni B., Hivon E., Bouchet F.R., Maffei B., 1998, MNRAS 295, 877

Hacking P., Houck J.R., 1987, ApJS 63, 311

Hauser M.G., Arendt R.G., Kelsall T., et al., 1998, ApJ 508, 25

Helou G., Beichman C.A., 1990, In: From Ground-Based to Space-Borne Sub-mm Astronomy, Proc. of the 29th Liége International Astrophysical Colloquium, ESA SP-314, p. 117

Herbstmeier U., Abraham P., Lemke D., et al., 1998, A&A 332, 739

Ishii T.T., Takeuchi T.T., Hirashita H., Yoshikawa K., 1999, In: Proc. of 33rd ESLAB Symp., Star Formation from the Small to the Large Scale. In press

Jahoda K., Lockman F.J., McCammon D., 1990, ApJ 354, 184

Kawara K., Sato Y., Matsuhara H., et al., 1998, A&A 336, L9(Paper I)

Kessler M.F., Steinz J.A., Anderegg M.E., et al., 1996, A&A 315, L27

Kirschner R.P., Oemler A., Schechter P.L., 1979, AJ 84, 951

Lagache G., Abergel A., Boulanger F., et al., 1999, A&A 344, 322

Lagache G., Puget J.L., 2000, A&A 355, 17, astro-ph/9910255

Lagache G., Haffner L.M., Reynolds R.J., Tufte S.L., 2000, A&A in press, astro-ph/9911355

Lemke D., Klaas U., Abolins J., et al., 1996, A&A 315, L64

Lockman F.J., Jahoda K., McCammon D., 1986, ApJ 302, 432

Lonsdale C.J., Hacking P.B., Conrow T.P., Rowan-Robinson M., 1990, ApJ 358, 60

Low F.J., Young E., Beintema D.A., et al., 1984, ApJ 278, L19

Müller T.G., 2000, In: Laureijs R.J., Leech K., Kessler M.F.(eds.) ISO beyond point sources: studies of extended infrared emission, SP-455, ESA Publications Division, ESA/ESTEC

Murakami H., 1998, Proc. SPIE 3356, 471

Puget J.L., Lagache G., Clements D.L., et al., 1999, A&A 345, 29

Rowan-Robinson M., Walker D., Chester T., Soifer T., Fairclough J., 1986, MNRAS 219, 273

Rowan-Robinson M., 1999, In: Lutz D., Tacconi L.(eds.) Ultraluminous Galaxies: Monsters or Babies? Ap&SS, astro-ph/9906308

Schmidt H.R., Kinney A.L., Calzeti D., Storchi-Bergmann T., 1997, AJ 144, 592

Takeuchi T.T, Hirashita H., Ohta K., et al., 1999, PASP 111, 288

Tan J.C., Silk J., Balland C., 1999, ApJ 522, 579

Taniguchi Y., Okuda H., Wakamatsu K., et al., 1994, In: Sato K.(ed.) Evolution of the Universe and its Observational Quest. Universal Academy Press, p. 545

Wheelock S., et al., 1994, IRAS Sky Survey Atlas Explanetary Supplement. JPL Publication 94-11